# Thermal Modeling and Analysis of Metal Foam Heat Sink with Thermal Equilibrium and Non-Equilibrium Models

## Yongtong Li[1], Liang Gong[1, *], Hui Lu[1], Dexin Zhang[1] and Bin Ding[1]

**Abstract:** In the present study, the thermal performance of metal foam heat sink was numerically investigated by adopting the local thermal non-equilibrium (LTNE) model and local thermal equilibrium (LTE) model. Temperature field distributions and temperature difference field distributions of solid and fluid phases were presented. Detailed thermal performance comparisons based on the LTE and LTNE models were evaluated by considering the effects of the relevant metal foam morphological and channel geometrical parameters. Results indicate that a distinct temperature difference exists between the solid and fluid phases when the LTNE effect is pronounced. The average Nusselt numbers predicted by both the LTE and LTNE models are approaching with the increase of porosity, pore density, Reynolds number, large thermal conductivity ratio, and large aspect ratio. This is attributed to the significant reduction of the interstitial convective thermal resistance between the solid and fluid phases, as a result, the LTE model can replace the LTNE model for thermal modeling in these conditions. In addition, the overall thermal performance assessment of metal foam heat sink is compared with the non-porous heat sink, and it shows that the thermal performance factor of metal foam heat sink is approximately two times of the non-porous heat sink.

**Keywords:** Metal foam, LTE and LTNE, heat transfer, numerical simulation.

## Nomenclature

$a_{sf}$     Specific area ($m^{-1}$)
$A$       Area ($m^2$)
$c_p$      Specific heat ($J \cdot kg^{-1} \cdot K^{-1}$)
$C_F$     Inertial coefficient
$D_h$     Hydraulic diameter (m)
$h_m$     Average heat transfer coefficient ($W \cdot m^{-2} \cdot K^{-1}$)
$h_{sf}$     Interfacial heat transfer coefficient ($W \cdot m^{-2} \cdot K^{-1}$)
$H_c$     Channel height (m)
$k$       Thermal conductivity ($W \cdot m^{-1} \cdot K^{-1}$)

$k_{fe}$      Effective fluid thermal conductivity ($W·m^{-1}·K^{-1}$)

$k_{se}$      Effective solid thermal conductivity ($W·m^{-1}·K^{-1}$)

$kr$      Thermal conductivity ratio($kr=k_f/k_s$)

$K$      Permeability ($m^2$)

$L$      Channel length (m)

$Nu_m$      Average Nusselt number

PPI      Pore density (pores per inch)

$pf$      Thermal performance factor

$q$      Heat flux ($W·m^{-2}$)

$r$      Aspect ratio ($r=H_c/W_c$)

$Re$      Reynolds number

$T_f$      Fluid temperature (K)

$T_{in}$      Fluid inlet temperature (K)

$W_c$      Channel width (m)

$W_r$      Rib width (m)

$u,v,w$      Velocity components ($m·s^{-1}$)

$x,y,z$      Cartesian coordinates (m)

**Greek symbols**

$\varepsilon$      Porosity

$\mu$      Dynamic viscosity ($kg·m^{-1}·s^{-1}$)

$\rho$      Density ($kg·m^{-3}$)

$\varepsilon_T$      Temperature control effectiveness

$\Delta$      Difference

**Subscripts**

eff      Effective

f      Fluid

fe      Fluid effective

p      Porous

in      Inlet

m      Average

max      Maximum

non      Non-porous

s      Solid

se      Solid effective

w      Wall

## 1 Introduction

With appealing thermal, electrical, acoustic and mechanical characteristics, metal foams have a promising future in varieties of industrial applications, including electronic heat

sinks, catalyst supports, fuel cells, solar energy applications, compact heat exchangers, etc. [Kolaczkowski, Awdry, Smith et al. (2016); Wang, Kong, Xu et al. (2019); Wang, Shuai, Tan et al. (2013); Abadi and Kim (2017)]. In particular, metal foams have excellent thermal advantages of large internal convection surface area per volume, high thermal conductivity, low relative density, and vigorous fluid mixing capability, which makes them competitive candidates for heat transfer enhancement. Therefore, the thermal transport mechanisms in metal foam need to be analyzed in theory, which in return will provide a guideline for thermal equipment design and optimization.

The volume-average technique for thermal modeling of convective heat transfer in metal foam primarily consists of two models. One is known as the local thermal equilibrium (LTE) model, in which the working fluid and foam ligament are treated as one phase and assumed to be the same temperature, which is a simplified heat transfer model with an artificial assumption of thermal equilibrium between solid and fluid phases. The other model is the local thermal non-equilibrium (LTNE) model, in which the temperature difference between the fluid and solid phases is considered. These two models are also referred to as the one energy model and the two-energy model, respectively. In the LTE model, there is one energy equation needed to be solved, and the effective thermal conductivity is the unique parameter being determined. Normally, it is calculated by means of the weighted arithmetic mean of the solid phase and fluid phase thermal conductivities, according to their occupied volume fractions. The LTNE model is referred to as the two-energy model, consisting of the fluid phase and the solid phase (solid matrix) energy equations. Compared to the LTE model, the numerical solution for the LTNE model is more complicated because the conjugated thermal transport between the fluid phase and the solid phase should be solved simultaneously. In addition, more parameters, including effective thermal conductivity [Boomsma and Poulikakos (2001); Singh and Kasana (2004); Dai, Nawaz, Park et al. (2010)], interfacial heat transfer coefficient [Calmidi and Mahajan (2000); Zhao, Lu and Tassou (2006); Saito and De Lemos (2006)], and the specific surface area [Calmidi and Mahajan (2000)], should be determined before simulations. Until now, both of the two models have been employed to investigate convective heat transfer in metal foam filled pipes, channels or heat sinks.

Bayomy et al. [Bayomy, Saghir and Yousefi (2016)] conducted a combined numerical and experimental study of the water-cooled aluminum foam heat sink for electronics cooling. In the numerical procedure, the assumption of local thermal equilibrium between the fluid and solid phase is adopted. Gong et al. [Gong, Han and Cheng (2001)] obtained the analytical solution of forced convection in a tube filled with porous media using the LTE model. Lee et al. [Lee and Vafai (1999)] investigated the validity of the LTE model and an error map is conceptually presented to assess the solid and fluid temperature difference. Hung et al. [Hung, Huang and Yan (2013a, 2013b)] numerically investigated the hydraulic and thermal performance of porous-microchannel heat sink with different porous configuration designs by using the LTE model.

However, some other studies addressed that the temperature between the solid and fluid phases is different, especially when the thermal conductivity difference between the solid and fluid phases is large. Thus, the LTNE model is employed instead of the LTE model for numerical simulations. Lu et al. [Lu, Zhao and Tassou (2006)] investigate the forced

convection characteristics in high porosity metal foam filled pipes with LTNE model. Calmidi et al. [Calmidi and Mahajan (2000)] experimentally and numerically studied the forced convention in metal foam, and the correlations of thermal dispersion conductivity and the interfacial heat transfer coefficient are obtained based on the experimental results. Shih et al. [Shih, Chiu and Hsieh (2006)] experimentally measured the solid and fluid temperatures along the metal foam height direction under imping air-jet condition for extracting temperature difference between them. Results show that the LTNE effect is obviously observed at the small foam height region or low Reynolds number. Yang et al. [Yang, Zeng, Wang et al. (2010)] numerically studied the forced convection in porous pin fin heat sink with the assumption of non-equilibrium heat transfer. It indicates that the long elliptic porous pin fin heat sink demonstrates the best thermal performance. In the previous literature of Xu et al. [Xu, Qu, Lu et al. (2011)], Zhao et al. [Zhao, Lu and Tassou (2006)], and Phanikumar et al. [Phanikumar and Mahajan (2002)], the parameter of solid to fluid thermal conductivity ratio ($k_s/k_f$) is used to evaluate the LTNE effect. However, Kim et al. [Kim and Jang (2002)] proposed a criterion for evaluating the LTNE effect in terms of Darcy number, Prandtl number, Reynolds number, and Nusselt number. More researches associated with the forced convection heat transfer in metal foam by considering the non-equilibrium heat transfer can be found in references [Shen, Yan, Sunden et al. (2017); Zhao, Kim, Lu et al. (2001); Chen, Huang and Hwang (2013); Li, Gong, Xu et al. (2017)].

As summarized above, it is known that both the LTE and LTNE models have been adopted to establish the energy equation for thermal modeling of convection heat transfer in metal foam. However, due to the complex metal foam three-dimensional geometry and intricate thermo-physical characteristics, a more general criterion accounting for in which conditions the LTE model can be used instead of LTNE model has not been proposed. Furthermore, few works have been conducted to systematically compare the thermal performance of metal foam heat sink by using the LTNE and LTE models.

In the present study, a systematic numerical analysis of thermal transport in metal foam heat sink by using the LTE and LTNE models is presented. The temperature fields of the solid phase and fluid phase and temperature difference fields between them are presented to demonstrate the non-equilibrium heat transfer characteristics. The thermal performances of metal foam heat sink obtained by the LTE and LTNE models, in terms of the average Nusselt number, temperature control effectiveness and thermal performance factor, are comprehensively compared by considering the effects of the relevant morphological and geometrical parameters. In addition, a thermal performance comparison between the metal foam heat sink and the non-porous channel is carried out to demonstrate the superiority of using metal foam in the thermal management of power electronics.

## 2 Physical model and mathematical formulation

### 2.1 Physical model

The physical model considered in the present study is illustrated in Fig. 1. Fig. 1(a) shows the overall view of the schematic diagram of the metal foam heat sink. High porosity metal foam is incorporated into the whole channel. To simply the numerical simulations and save the computing resource, a single computation domain is employed, with a

dimension of 2.4 mm×7 mm×20 mm in the *x, y* and *z*-direction, as shown in Fig. 1(b). The width of the fin is $W_r$ (0.2 mm), and the thicknesses of the top cover plate and the bottom substrate are $\delta_1$ (0.5 mm) and $\delta_2$ (0.5 mm), respectively. The fluid flows into the computational domain with a uniform temperature $T_0$ and velocity $u_{in}$. Constant heat flux is supplied at the bottom wall to simulate the rejected waste heat from the electronics. The related parameters are listed in Tab. 1.

To simplify the numerical analysis, several assumptions are considered. (1) The flow is assumed to be steady, laminar, and incompressible; (2) Metal foam has homogenous porosity and pore size; (3) The thermo-physical properties of the fluid and metal foam are independent on the variation of the temperature; (4) Metal foam is bonded very well into the channel to reduce the thermal contact resistance.
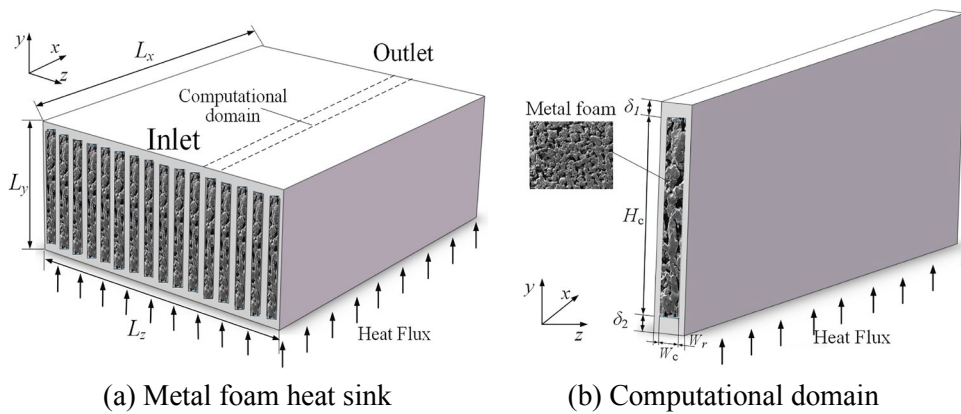


(a) Metal foam heat sink      (b) Computational domain

**Figure 1:** Schematic diagram of (a) metal foam heat sink and (b) computational domain

**Table 1:** Parameters used in the numerical simulations

| Parameter | Value range | Unit |
|---|---|---|
| Porosity | 0.8~0.99 | 1 |
| Channel width $W_c$ | 2 | mm |
| Channel height $H_c$ | 6 | mm |
| Channel length $L_x$ | 20 | mm |
| Thickness of substrate $\delta_1$ | 0.5 | mm |
| Thickness of substrate $\delta_2$ | 0.5 | mm |
| Thickness of wall $W_r$ | 0.2 | mm |
| Heat flux $q$ | 100 | W/cm$^2$ |
| Reynolds number $Re$ | 100-1000 | 1 |

### 2.2 Mathematical formulation

Based on the assumptions, the volume-average technique is adopted to solve the forced convection heat transfer details. The Forchheimer-Brinkman extended Darcy model is

adopted for describing the fluid flow characteristics. The LTE and LTNE models are utilized for modeling the thermal transport in the metal foam region, respectively. The corresponding governing equations can be written as follows:

Continuity equation

$$\nabla \cdot V = 0 \tag{1}$$

Momentum equation:

$$\frac{\rho_f}{\varepsilon^2}(V \cdot \nabla)V = -\nabla p_f + \mu_{f,eff}\nabla^2 V - (\frac{\mu_f}{K} + \frac{\rho_f C_F}{\sqrt{K}}|V|)V \tag{2}$$

Energy equation

(a) LTE model

$$(\varepsilon \rho c_p)(V \cdot \nabla T) = k_{eff}\nabla^2 T \tag{3}$$

(b) LTNE model

Fluid phase energy equation:

$$(\rho c_p)_f(V \cdot \nabla T_f^f) = \nabla \cdot (\varepsilon k_f \nabla T_f^f) + h_{sf}a_{sf}(T_s^s - T_f^f) \tag{4}$$

Solid matrix energy equation:

$$(1-\varepsilon)k_s\nabla^2 T_s^s - h_{sf}a_{sf}(T_s^s - T_f^f) = 0 \tag{5}$$

where $c_p$, $\mu_{f,eff}$, $\varepsilon$, $T_f^f$, $T_s^s$ are the specific heat, effective dynamic viscosity, porosity, fluid phase temperature and solid phase temperature, respectively; $a_{sf}$, $C_F$, $k_s$, $K$, $h_{sf}$ are the surface area density, inertial coefficient, solid material thermal conductivity, permeability and interstitial heat transfer coefficient, respectively. The correlations of these parameters can be found in the previous research [Li, Gong, Xu et al. (2017)].

In numerical simulations, it is assumed that the metal foam heat sink is packed on the top of a high-power electronics with the generated heat flux of 100 W/cm². Symmetry boundary conditions are adopted for the two-side walls, the top wall and the rest of the walls are set as adiabatic. At the interfaces of metal foam and internal surface walls, continuous temperature and heat flux boundary conditions are adopted for modeling the conjugated heat transfer, and the non-slip boundary condition is applied for solving the momentum equation. The fluid flows into the channel with uniform velocity and constant temperature. The corresponding boundary conditions are mathematically expressed as follows:

(1) At the inlet ($x=0$):

$u=u_{in}$, $T=T_{in}$, $w=v=0$ $\tag{6}$

(2) At the bottom ($y=0$):

$$-k_s\frac{\partial T_s}{\partial y} = q_w \tag{7}$$

(3) At the outlet ($x=L$):

$$\frac{\partial T_f^f}{\partial x} = \frac{\partial T_s^s}{\partial x} = \frac{\partial T}{\partial x} = 0, \frac{\partial u}{\partial x} = \frac{\partial v}{\partial x} = \frac{\partial w}{\partial x} = 0 \tag{8}$$

(4) At the inside wetted walls [Feng, Kuang, Wen et al. (2014)]:

$$-k_{se}\frac{\partial T_s^s}{\partial n} - k_{fe}\frac{\partial T_f^f}{\partial n} = -k_s\frac{\partial T_s}{\partial n}, T_s^s = T_f^f = T \tag{9}$$

(5) At the other outside walls:

$$-k_s\frac{\partial T_s}{\partial n} = 0 \tag{10}$$

### 2.3 Evaluation of performance parameters

The thermal performance evaluation is based on the average Nusselt number ($Nu_m$). The comparison of the average Nusselt number obtained by the LTE and LTNE models is paid much attention to examine the non-equilibrium effect. The $Nu_m$ is defined as:

$$Nu_m = \frac{h_m D_h}{k_f} = \frac{q_w D_h}{(T_{w,m} - T_f)k_f} \tag{11}$$

where the $q_w$ is the applied heat flux; $D_h$ is the hydraulic diameter of the channel, $D_h = 4H_c W_c/2(H_c + W_c)$; $T_{w,m}$ is the average temperature of the bottom wall; $T_f$ is the average fluid temperature; $k_f$ is the fluid thermal conductivity.

The flow resistance of the heat sink is characterized by the friction factor, given as:

$$f = \frac{(\Delta p / L)D_h}{1/2\rho u^2} \tag{12}$$

The effective control of the maximum temperature is of great significance, especially in the application of electronic cooling. In order to compare the temperature control capability of metal foam heat sink with the non-porous heat sink, the temperature control effectiveness [Hung, Huang and Yan (2013a)] is adopted, as shown:

$$\varepsilon_T = 1 - \frac{(T_{w,max} - T_{in})_p}{(T_{w,max} - T_{in})_{non}} \tag{13}$$

The overall thermal assessment of the metal foam heat sink is compared with the non-porous channel in terms of thermal performance factor, which is evaluated based on the enhancement in heat transfer versus the corresponding flow resistance, defined as Yang et al. [Yang, Zeng, Wang et al. (2010)]:

$$pf = \frac{Nu_{m,p} / Nu_{m,non}}{(f_{m,p} / f_{m,non})^{1/3}} \tag{14}$$

where the $Nu_{m,p}$ and $f_{m,p}$ are the average Nusselt number and friction factor of the metal foam channel, respectively. $Nu_{m,non}$ and $f_{m,non}$ are the average Nusselt number and friction factor of the non-porous channel, respectively.

### 3 Grid independence test and numerical method validation

The governing equations for the computational domain are solved by the finite-volume method. The continuity and the momentum equations are solved iteratively. The numerical results are recognized as being convergent when the relative errors of momentum and energy

equations between two successive iterations are less than $10^{-6}$ and $10^{-8}$, respectively.

To make sure the computational results are independent of the grid size, the grid independence test is performed by examining the effect of grid size on the average temperature of the heated wall and pressure drop. The results obtained from the grids of $10\times40\times80$ and $35\times70\times140$ (in *x*, *y* and *z*-direction) indicates that the differences in average temperature and pressure drop are within 1.65% and 3.48%, respectively. However, the relative errors are reduced to 0.30% and 0.7% by using the grids of $30\times70\times140$ and $50\times100\times180$. Finally, all the computations are based on the $35\times70\times140$ grid system.

The reliability of the present numerical model is also validated by comparing the present results with the previous research. The measured pressure drop through aluminum foam reported in Garrity et al. [Garrity, Klausner and Mei (2010)] and the numerical results of the overall heat transfer rate in Feng et al. [Feng, Kuang, Wen et al. (2014)] are employed for comparison, as shown in Fig. 2. Fig. 2(a) shows the comparison of the pressure drop, which shows good agreement. The numerical model for thermal behavior prediction is depicted in Fig. 2(b), which also matches well with the previous results, with the maximum deviation of 13% at the velocity of 1 m/s. The deviations may result from the errors of extracting the interfacial heat transfer coefficients and foam thermal conductivity. Accordingly, it is suitable to use the present numerical method to carry out simulations.
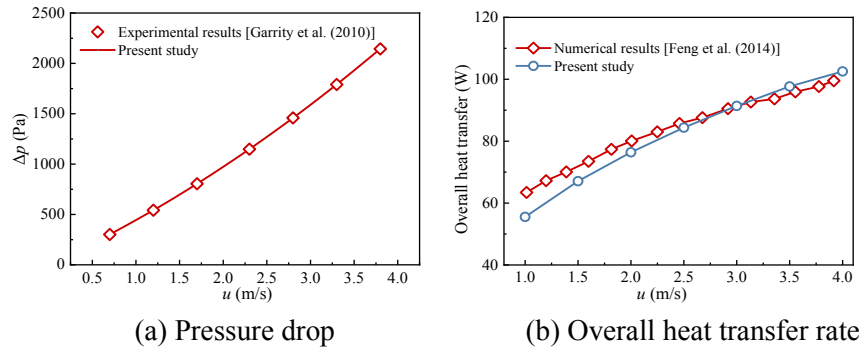


(a) Pressure drop          (b) Overall heat transfer rate

**Figure 2:** Model validation (a) pressure drop and (b) overall heat transfer rate

## 4 Result and discussion

The following section primarily focuses on analyzing the non-equilibrium heat transfer characteristics associated with the relevant geometrical and morphological parameters. In addition, the temperature control effectiveness and the overall thermal performance assessment of metal foam heat sink are compared with the empty channel.

### *4.1 Temperature filed distributions*

The Forchheimer extended Darcy momentum equation has been applied together with the LTE or LTNE model for modeling the flow and heat transfer in metal foam heat sink. To demonstrate the local thermal non-equilibrium heat transfer between the fluid and solid phases, the temperature profiles of the solid and fluid phases in two different lines (*x*=5

mm and 15 mm) along the channel height direction are presented in Fig. 3. It is noted that the temperatures of fluid and solid phases are decreasing along the heigh direction because the heat flux is applied at the bottom of the channel. In addition, there exists a distinct temperature difference between the solid and fluid phases, with solid phase temperature higher than the fluid phase, demonstrating the existence of local non-equilibrium heat transfer between the metal foam matrix and the fluid. It is notable that the temperature difference between the solid and fluid phases is larger when the dimensionless channel height is smaller than 0.4 (in LTNE state), beyond which temperature difference between the solid and fluid phases is marginal, thus the metal foam matrix and the fluid are in the LTE state.
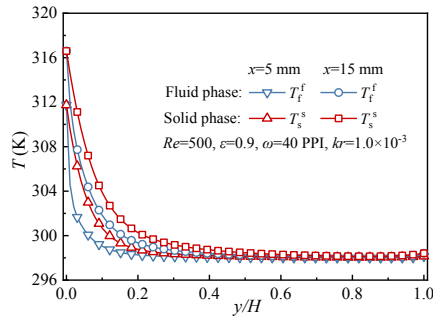


**Figure 3:** Temperature profiles along with channel height

In light of the large thermal conductivity difference between the foam ligament and fluid, much attention should be paid to the non-equilibrium heat transfer within metal foam. The temperature field distributions predicted by LTE and LTNE models, for two thermal conductivity ratios ($kr=k_f/k_s$) of $10^{-4}$ and $10^{-5}$, are shown in Fig. 4. From the comparison of Figs. 4(b) and 4(c), Figs. 4(e) and 4(f), it is pointed out that a pronounced temperature difference is presented between the solid and fluid phases, and the solid phase temperature is higher than the fluid phase. It is also noted that the smaller the thermal conductivity ratio is, i.e., the thermal conductivity difference between solid and fluid phases is large, the more distinct temperature difference between them. Additionally, the temperature distribution of Figs. 4(a) and 4(d) predicted by the LTE model is higher in comparison with Figs. 4(b) and 4(e), respectively.
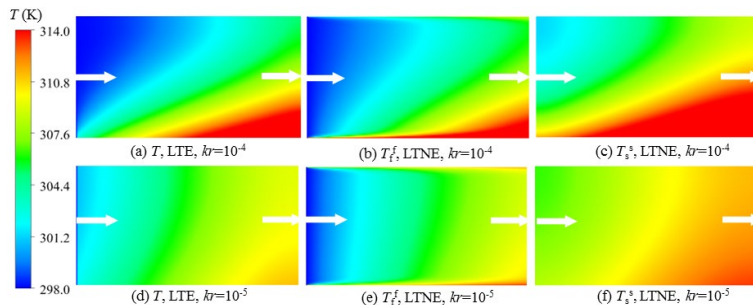


**Figure 4:** Temperature field distributions along the central *x-y* cross-section for two

thermal conductivity ratios

## *4.2 Temperature difference field distributions*

The non-equilibrium heat transfer performance is also presented in terms of the temperature difference filed distributions, by considering the relevant parameters including pore density, porosity, Reynolds number (*Re*) and aspect ratio (*r*), as shown in Figs. 5-8.

In Fig. 5, it indicates that the temperature difference between the solid and fluid phases for 15 PPI is much higher than that of 50 PPI, which implies that the LTNE effect can be decreased by increasing pore density. It is attributed to that increasing the pore density would increase the internal convection surface area, promoting the convective heat transfer between solid matrix and fluid. Fig. 6 presents the temperature difference field distributions for porosities of 0.8 and 0.95, respectively. The temperature difference is higher in a smaller porosity of 0.8, in comparison with a larger porosity of 0.95. The foam ligament volume in the channel decreases with increasing foam porosity, leading to the solid phase temperatures approaches the fluid phase temperature due to fewer solid material in the channel. Therefore, the fluid and solid phases are approaching to LTE state.
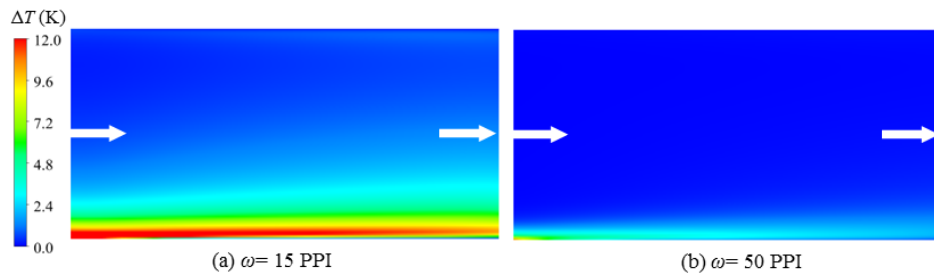


(a) $\omega$= 15 PPI                                             (b) $\omega$= 50 PPI

**Figure 5:** The temperature difference fields for two pore densities



(a) $\varepsilon$=0.8                                                 (b) $\varepsilon$= 0.95
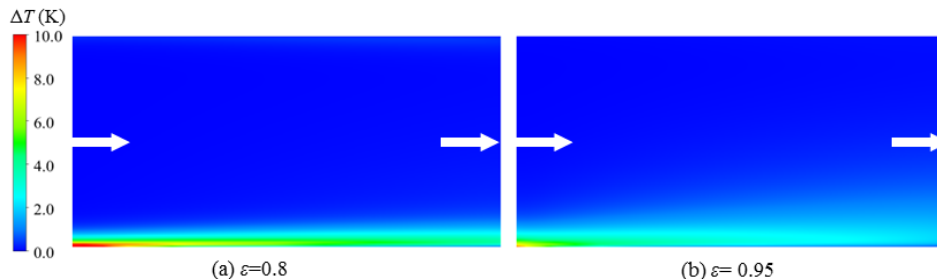
**Figure 6:** The temperature difference fields for two porosities

The effects of inlet velocity (corresponding to the *Re*) on temperature difference filed distributions are shown in Fig. 7. Increasing *Re* would enhance the interfacial heat transfer coefficient and lower the local convective heat transfer resistance between the solid matrix and fluid, as a result, a reduction of the temperature difference between the solid and fluid phases is attained. Fig. 8 shows the effects of the channel aspect ratio ($r=H_c/W_c$) on the

temperature difference field distribution. The temperature difference between the solid and fluid phases is higher for a smaller aspect ratio, demonstrating that the LTNE effect is more pronounced. Accordingly, the implementation of LTNE is necessary for accurately modeling heat transfer within metal foam heat sink with a small aspect ratio.
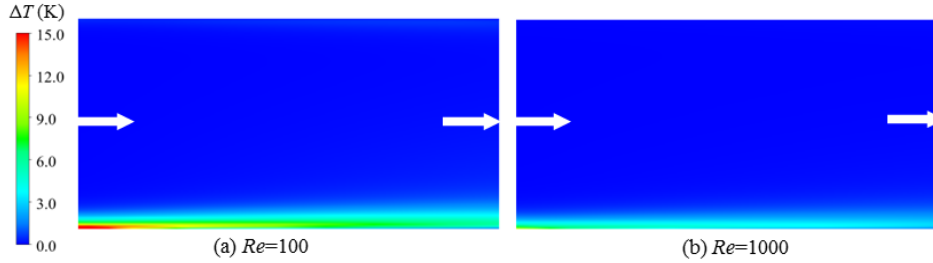


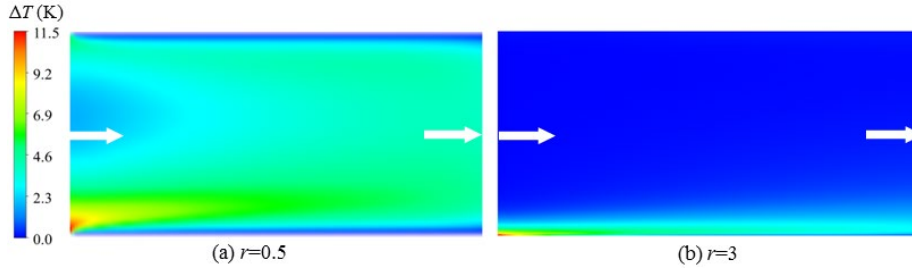**Figure 7:** The temperature difference fields for two *Re*



**Figure 8:** The temperature difference fields for two aspect ratios

### 4.3 Thermal performance comparison with LTE and LTNE models

Fig. 9 plots the comparison of thermal performance predicted by the LTE and LTNE models for various *Re*. The average Nusselt number ($Nu_m$) of LTE and LTNE models with *Re* is shown in Fig. 9(a). As expected, the $Nu_m$ of LTE and LTNE models show a monotonic increase with *Re*, resulted from the enhanced heat transfer coefficient. It also illustrates that the $Nu_m$ of LTE model is larger than that of the LTNE model. Because the temperatures of the solid and fluid phases are assumed in thermal equilibrium state in the LTE model, i.e., the convective heat transfer resistance between the solid matrix and fluid interface is ignored, leading to the overestimated convective heat transfer performance. However, the temperature difference between the solid and fluid phases is considered in LTNE model, which introduces the interstitial convection thermal resistance and produces a lower $Nu_m$. Fig. 9(b) presents that the average temperature ($T_m$) of LTE model, and the solid ($T_{m,s}$) and fluid ($T_{m,f}$) phases temperature of the LTNE model at the central *x-y* cross-section decrease with the increase of *Re*. In addition, the temperature difference ($\Delta T_m$) between the solid and fluid phases is also declined with *Re*, which would result in a LTE state with increasing of *Re*. The temperature difference $\Delta T_m$ is decreasing from 1.28 K to 0.26 K in the entire range of *Re*.

(a) Effect of $Re$ on $Nu_m$        (b) Effect of $Re$ on temperature
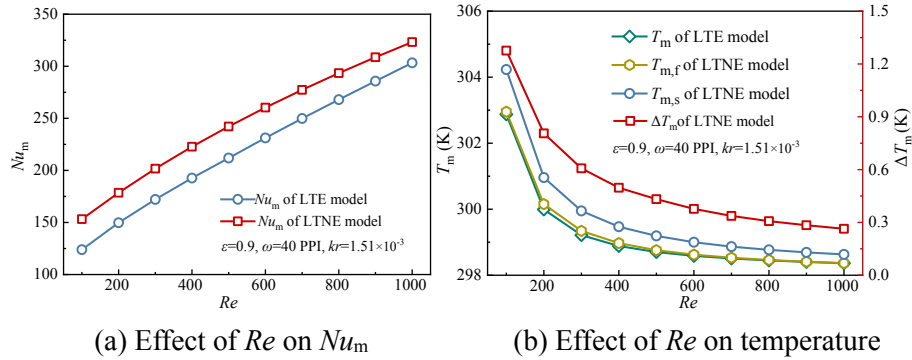
**Figure 9:** Effects of $Re$ on heat transfer with LTE and LTNE models

The variation of $Nu_m$ of the LTE and LTNE models with porosity is plotted in Fig. 10. Results reveal that the $Nu_m$ exhibits a significant decrease with porosity, as shown in Fig. 10(a). The $Nu_m$ predicted by the LTE and LTNE models are approaching with the increase of porosity, which is proved that the LTE state would be achieved. In this circumstance, the LTE model can be used instead of LTNE model for thermal analysis. Variations of average temperature and the temperature difference between the solid and fluid phases are shown in Fig. 10(b). The $T_m$ of LTE model, and the $T_{m,s}$ and $T_{m,f}$ of the LTNE model decrease with porosity. Meantime, the heat transfer performance would be weakened due to the sharply decreased effective thermal conductivity. It is noted that the temperature difference between the solid and fluid phases could be neglected at the porosity of 0.98, approximately 0.1 K. This indicates that the solid and fluid phases are closing to a LTE state, thus the LTE model can be used instead of the LTNE model in this condition.
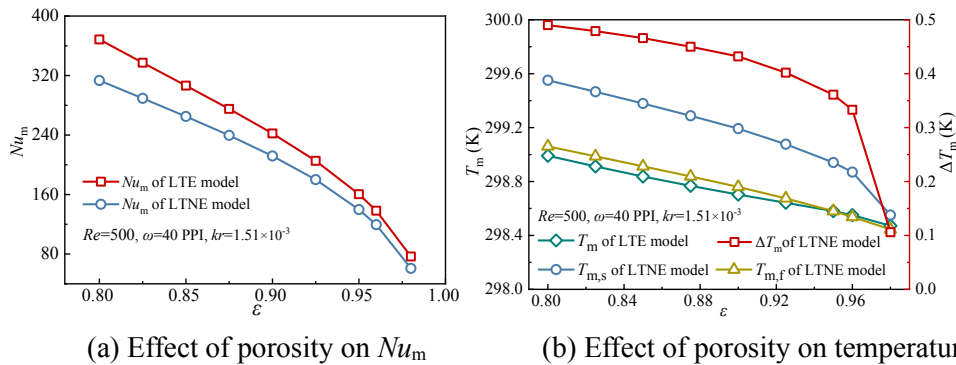


(a) Effect of porosity on $Nu_m$        (b) Effect of porosity on temperature

**Figure 10:** Effects of porosity on heat transfer with LTE and LTNE models

The effects of pore density on the $Nu_m$ for the LTE and LTNE models are shown in Fig. 11. It is seen from Fig. 11(a) that the $Nu_m$ obtained by the LTNE shows a significant increase with pore density. The enhanced heat transfer performance is resulted from the dramatically increased internal convective heat transfer surface area. On the contrary, the $Nu_m$ of LTE model shows a relatively small variation with pore density. The $Nu_m$ of the two models is tended to reach the same value at high pore density, which implies that the

heat transfer performance predicted by the LTE and LTNE models is becoming identical with increasing pore density. Therefore, the thermal performance obtained from the LTE and LTNE models would be the same at high pore density, while the difference between them should be mainly emphasized in lower pore density. Fig. 11(b) shows that the $T_m$ of LTE model, $T_{m,s}$ and $T_{m,f}$ of LTNE model, as well as the $\Delta T_m$ reduce with increasing pore density. For instance, the $\Delta T_m$ declines from 2.2 K to 0.2 K.



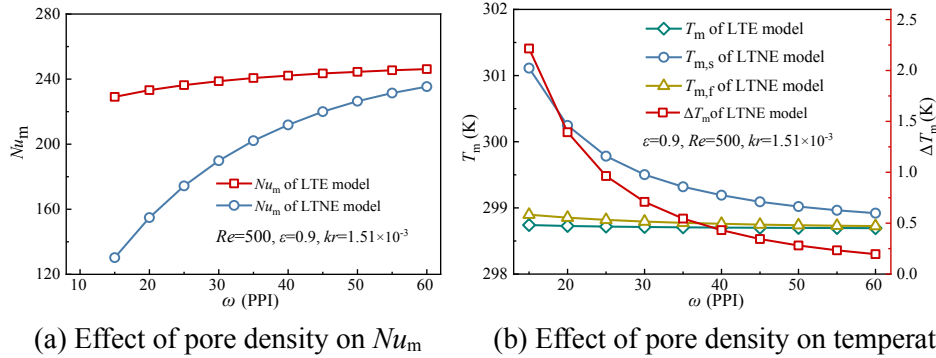(a) Effect of pore density on $Nu_m$     (b) Effect of pore density on temperature

**Figure 11:** Effects of pore density on heat transfer with LTE and LTNE models

The thermal conductivity difference between the solid and fluid phases is the key parameter influencing the non-equilibrium heat transfer. Fig. 12(a) shows the $Nu_m$ of LTE and LTNE models *vs.* thermal conductivity ratio ($kr$). It reveals that the $Nu_m$ of LTE and LTNE models both decrease, and the difference between the two models is gradually reduced with the increase of $kr$. In particular, when the thermal conductivity ratio is 1, which means that the thermal conductivities of the fluid and solid phases are equal. In such a case, the solid and fluid phases are in the LTE state, and the resulting $Nu_m$ of LTE and LTNE models would be the same. As presented Fig. 12(b), the $T_m$, $T_{m,s}$ and $T_{m,f}$, as well as the $\Delta T_m$ decrease with increasing of $kr$. It is noteworthy that the $\Delta T_m$ between the solid and fluid phases is zero when $kr$ is equal to 1, because the solid matrix and fluid are in the LTE state. The above results suggest that the LTE can be utilized instead of the LTNE model when thermal conductivity difference of the solid and fluid phases is small.
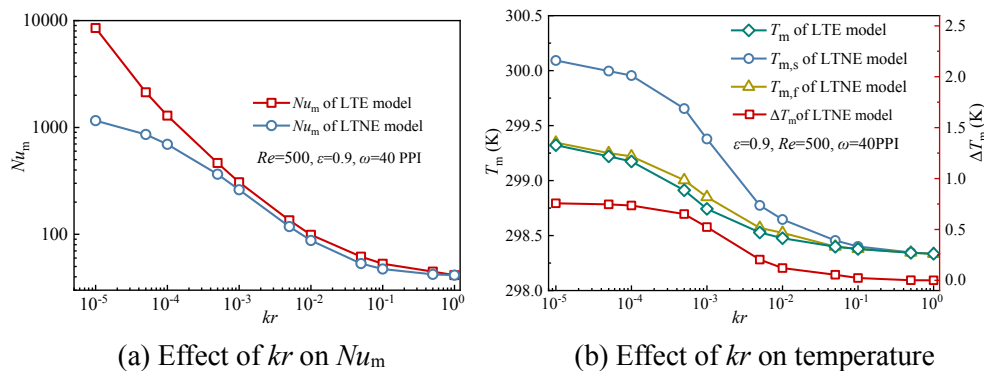


(a) Effect of $kr$ on $Nu_m$     (b) Effect of $kr$ on temperature

**Figure 12:** Effects of pore density on heat transfer with LTE and LTNE models

The non-equilibrium heat transfer between the solid and fluid phases is also evaluated by considering the effects of channel geometrical parameters, in terms of the aspect ratio. Fig. 13(a) shows that the increase of the aspect ratio increases $Nu_m$, because the amount of working coolant increases with aspect ratio, leading to the improved convective heat transfer performance. The $Nu_m$ of the two models shows a relatively large difference at smaller aspect ratio, which is becoming small with the increase of aspect ratio. This implies that the non-equilibrium heat transfer should be emphasized at a low aspect ratio. Fig. 13(b) indicates that the $T_m$ of LTE model, the $T_{m,s}$ and $T_{m,f}$ of the LTNE model, and the $\Delta T_m$ of the LTNE model exhibit a decreasing trend with aspect ratio. It is convinced that the temperature profile predicted by the LTE and LTNE models would be the same at a high aspect ratio. It confirms that the LTE can be adopted for thermal modeling at a high aspect ratio.
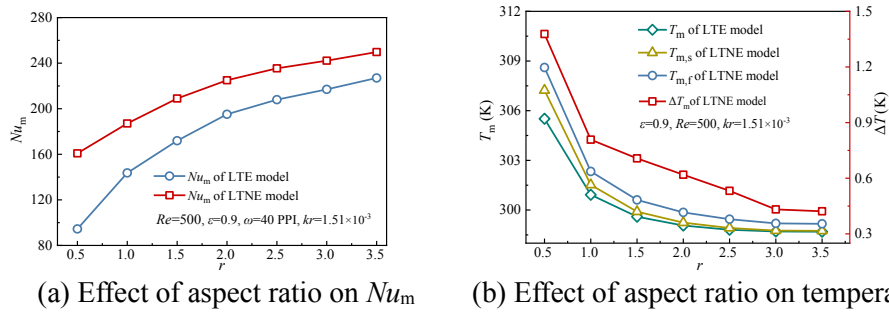


(a) Effect of aspect ratio on $Nu_m$    (b) Effect of aspect ratio on temperature

**Figure 13:** Effects of aspect ratio on heat transfer with LTE and LTNE models

### 4.4 Thermal performance comparison with non-porous channel

The effectiveness of metal foam heat sink for suppressing wall temperature is evaluated by using the temperature control effectiveness ($\varepsilon_T$). Compared with the empty channel, the effectiveness of maximum temperature control is better when $\varepsilon_T$ is larger than zero. Besides, a larger value of $\varepsilon_T$ leads to better temperature suppression. Fig. 14 shows that the $\varepsilon_T$ values are greater than 0 in the entire ranges of $Re$, indicating that the metal foam heat sink provides a better temperature suppression capability compared with the non-porous channel. Besides, the results reveal that the $\varepsilon_T$ of LTE model is larger than the LTNE model, because the interfacial convective thermal resistance between the solid and fluid phases is neglected, which results in an overestimated thermal performance.
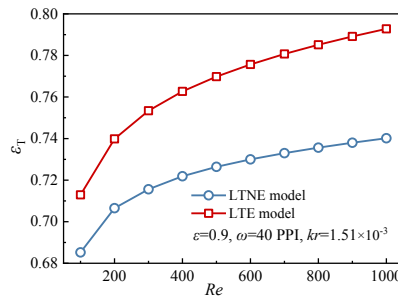


**Figure 14:** The temperature control effectiveness with $Re$

Metal foam heat sink provides a favorable heat transfer performance, however, which is accompanied by the high-pressure drop as a penalty. The thermal performance improvement compared with the non-porous channel is further evaluated by using the thermal performance factor (*pf*), as shown in Fig. 15. The *pf* exhibits a decreasing trend with increasing of *Re*, which is resulted from the dramatically increased flow resistance with increasing of the inlet velocity. The *pf* of LTE model is larger than the LTNE model, thus the implementation of LTE provides an overestimated evaluation of the thermal performance of metal foam heat sink. In addition, it is noteworthy that the *pf* values are greater than 1.0 for both models, meaning the metal foam heat sink has a higher convection performance.
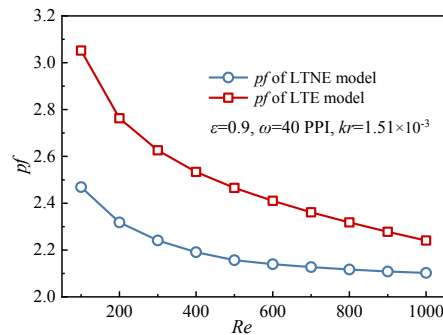


**Figure 15:** The thermal performance factor with *Re*

## 5 Conclusions

In this paper, thermal modeling of convection heat transfer within metal foam heat sink is numerically examined by using the LTE and LTNE models. The temperature profile, temperature field distributions, temperature difference field distributions, and average Nusselt number predicted by the two models are comprehensively compared and analyzed. The effects of relevant metal foam morphological and geometrical parameters, including porosity, pore density, Reynolds number, thermal conductivity ratio, and aspect ratio, are discussed in detail. Moreover, the thermal performance of the metal foam heat sink is compared with the non-porous heat sink. The following conclusions can be drawn:

(1) The implementation of LTE and LTNE models deduces different temperature or temperature difference field distributions. The non-equilibrium heat transfer should be emphasized when the LTNE effect is pronounced.

(2) The thermal non-equilibrium effect between the solid and fluid phases would be alleviated in the conditions of high porosity, large pore density, high Reynolds number, low thermal conductivity ratio, and large aspect ratio.

(3) When the local heat transfer thermal resistance between the solid and fluid phases is marginal, the LTE model can be employed instead of the LTNE model for thermal analysis with the advantage of convenient implementation.

(4) Compared with the non-porous channel, the metal foam heat sink can significantly enhance the cooling performance. The temperature control effectiveness is improved by

more than 70%. Also, the thermal performance factor is more than 2 times of the non-porous heat sink, indicating that the metal foam channel has better thermal performance.

**Conflicts of Interest:** The authors declare that they have no conflicts of interest to report regarding the present study.

**References**

**Abadi, G. B.; Kim, K. C.** (2017): Experimental heat transfer and pressure drop in a metal-foam-filled tube heat exchanger. *Experimental Thermal and Fluid Science*, vol. 82, pp. 42-49.

**Bayomy, A. M.; Saghir, M. Z.; Yousefi, T.** (2016): Electronic cooling using water flow in aluminum metal foam heat sink: experimental and numerical approach. *International Journal of Thermal Sciences*, vol. 109, pp. 182-200.

**Boomsma, K.; Poulikakos, D.** (2001): On the effective thermal conductivity of a three-dimensionally structured fluid-saturated metal foam. *International Journal of Heat and Mass Transfer*, vol. 44, no. 4, pp. 827-836.

**Calmidi, V. V.; Mahajan, R. L.** (2000): Forced convection in high porosity metal foams. *Journal of Heat Transfer*, vol. 122, no. 3, pp. 557-565.

**Chen, C. C.; Huang, P. C.; Hwang, H. Y.** (2013): Enhanced forced convective cooling of heat sources by metal-foam porous layers. *International Journal of Heat and Mass Transfer*, vol. 58, no. 1, pp. 356-373.

**Dyga, R.; Witczak, S.** (2012): Investigation of effective thermal conductivity aluminum foams. *Procedia Engineering*, vol. 42, pp. 1088-1099.

**Dai, Z.; Nawaz, K.; Park, Y. G.; Bock, J.; Jacobi, A. M.** (2010): Correcting and extending the Boomsma-Poulikakos effective thermal conductivity model for three-dimensional, fluid-saturated metal foams. *International Communications in Heat and Mass Transfer*, vol. 37, no. 6, pp. 575-580.

**Feng, S. S.; Kuang, J. J.; Wen, T.; Lu, T. J.; Ichimiya, K.** (2014): An experimental and numerical study of finned metal foam heat sinks under impinging air jet cooling. *International Journal of Heat and Mass Transfer*, vol. 77, pp. 1063-1074.

**Garrity, P. T.; Klausner, J. F.; Mei, R.** (2010): Performance of aluminum and carbon foams for air side heat transfer augmentation. *Journal of Heat Transfer*, vol. 132, no. 12, pp. 121901.

**Gong, W. P.; Han, J. T.; Cheng, F.** (2001): Theoretical study of heat transfer enhancement in pipe with porous body. *Journal of Hydrodynamics, Series B*, vol. 1, pp. 111-116.

**Hung, T. C.; Huang, Y. X.; Yan, W. M.** (2013): Thermal performance analysis of porous-microchannel heat sinks with different configuration designs. *International Journal of Heat and Mass Transfer*, vol. 66, pp. 235-243.

**Hung, T. C.; Huang, Y. X.; Yan, W. M.** (2013): Thermal performance of porous microchannel heat sink: effects of enlarging channel outlet. *International Communications in Heat and Mass Transfer*, vol. 48, pp. 86-92.

**Kim, S. J.; Jang, S. P.** (2002): Effects of the Darcy number, the Prandtl number, and the Reynolds number on local thermal non-equilibrium. *International Journal of Heat and Mass Transfer*, vol. 45, no. 19, pp. 3885-3896.

**Kolaczkowski, S. T.; Awdry, S.; Smith, T.; Thomas, D.; Torkuhl, L. et al.** (2016): Potential for metal foams to act as structured catalyst supports in fixed-bed reactors. *Catalysis Today*, vol. 273, pp. 221-233.

**Lee, D. Y.; Vafai, K.** (1999): Analytical characterization and conceptual assessment of solid and fluid temperature differentials in porous media. *International Journal of Heat and Mass Transfer*, vol. 42, no. 3, pp. 423-435.

**Li, Y.; Gong, L.; Xu, M.; Joshi, Y.** (2017): Thermal performance analysis of biporous metal foam heat sink. *Journal of Heat Transfer*, vol. 139, no. 5, pp. 052005.

**Phanikumar, M. S.; Mahajan, R. L.** (2002): Non-darcy natural convection in high porosity metal foams. *International Journal of Heat and Mass Transfer*, vol. 45, no. 18, pp. 3781-3793.

**Saito, M. B.; De Lemos, M. J.** (2006): A correlation for interfacial heat transfer coefficient for turbulent flow over an array of square rods. *Journal of Heat Transfer*, vol. 128, no. 5, pp. 444-452.

**Shen, B.; Yan, H.; Sunden, B.; Xue, H.; Xie, G.** (2017): Forced convection and heat transfer of water-cooled microchannel heat sinks with various structured metal foams. *International Journal of Heat and Mass Transfer*, vol. 113, pp. 1043-1053.

**Shih, W. H.; Chiu, W. C.; Hsieh, W. H.** (2006): Height effect on heat-transfer characteristics of aluminum-foam heat sinks. *Journal of Heat Transfer*, vol. 128, no. 6, pp. 530-537.

**Singh, R.; Kasana, H. S.** (2004): Computational aspects of effective thermal conductivity of highly porous metal foams. *Applied Thermal Engineering*, vol. 24, no. 13, pp. 1841-1849.

**Wang, F.; Shuai, Y.; Tan, H. P.; Yu, C.** (2013): Thermal performance analysis of porous media receiver with concentrated solar irradiation. *International Journal of Heat and Mass Transfer*, vol. 6, pp. 247-254.

**Wang, J., Kong, H.; Xu, Y. B.; Wu, J.** (2019): Experimental investigation of heat transfer and flow characteristics in finned copper foam heat sinks subjected to jet impingement cooling. *Applied Energy*, vol. 241, pp. 433-443.

**Xu, H. J.; Qu, Z. G.; Lu, T. J.; He, Y. L.; Tao, W. Q.** (2011): Thermal modeling of forced convection in a parallel-plate channel partially filled with metallic foams. *Journal of Heat Transfer*, vol. 133, no. 9, pp. 092603.

**Yang, J.; Zeng, M.; Wang, Q.; Nakayama, A.** (2010): Forced convection heat transfer enhancement by porous pin fins in rectangular channels. *Journal of Heat Transfer*, vol. 132, no. 5, pp. 051702.

**Zhao, C. Y.; Kim, T.; Lu, T. J; Hodson, H. P.** (2001): Thermal transport phenomenon in porvair metal foam and sintered beds. University of Cambridge, Final Report.

**Zhao, C. Y.; Lu, W.; Tassou, S. A.** (2006): Thermal analysis on metal-foam filled heat exchangers. Part II: Tube heat exchangers. *International Journal of Heat and Mass Transfer*, vol. 49, no. 15, pp. 2762-2770.